Journal of Machine Engineering, 2024, Vol. 24, No. 1, 103–117
ISSN 1895-7595 (Print) ISSN 2391-8071 (Online)

Received: *01 February 2024* / Accepted: *13 March 2024* / Published online: *19 March 2024*

additive manufacturing,
extrusion-based 3D bioprinting,
machine learning modelling

Javier ARDUENGO[1*], Nicolas HASCOET[2],
Francisco CHINESTA[2], Jean-Yves HASCOET[1]

OPEN-LOOP CONTROL SYSTEM FOR HIGH PRECISION EXTRUSION-BASED BIOPRINTING THROUGH MACHINE LEARNING MODELLING

Bioprinting is a process that uses 3D printing techniques to combine cells, growth factors, and biomaterials to create biomedical components, often with the aim of imitating natural tissue characteristics. Typically, 3D bioprinting adopts a layer-by-layer method, using materials known as bio-inks to build structures resembling tissues. This study introduces an open-loop control system designed to improve the accuracy of extrusion-based bioprinting techniques, which is composed of a specific experimental setup and a series of algorithms and models. Firstly, a method employing Logistic Regression is used to select the tests that will serve to train and test the following model. Then, using a Machine Learning Algorithm, a model that allows the optimization of printing parameters and enables process control through an open-loop system was developed. Through rigorous experimentation and validation, it is shown that the model exhibits a high degree of accuracy in independent tests. Thus, the control system offers predictability and adaptability capabilities to ensure the consistent production of high-quality bioprinted structures. Experimental results confirm the efficacy of this machine learning model and the open-loop control system in achieving optimal bioprinting outcomes.

1. INTRODUCTION

3D Bioprinting, also known as Additive Biomanufacturing, is a process that involves positioning biomaterials and living cells layer by layer to create engineered tissues and organs in 3D, preserving cellular viability [1]. Bioinks, used in bioprinting, consist of natural or synthetic biomaterials mixed with living cells. They come in two main types: cell-based bioinks with live cells alone or hydrogel-based bioinks combined with cell-laden natural, synthetic, or decellularized tissue hydrogels. Coupled with post-processing to ensure the maturing of the living construct, the potential applications for bioprinting includes [2]: in vitro 3D tissue/organ models for drug screening, organ development, toxicological, cosmetic research, etc., and tailoring of living structures for clinical transplantation or tissue repair.

[1] Nantes Université, Ecole Centrale Nantes, CNRS, GeM, UMR 6183, F-44000, Nantes, France
[2] PIMM, Arts et Métiers Institute of Technology, CNRS - UMR 8006, F-75013, Paris, France
[*] E-mail: javier.arduengo-garcia@ec-nantes.fr, nicolas.hascoet@ensam.eu,
franciso.chinesta@ensam.eu, jean-yves.hascoet@ec-nantes.fr
https://doi.org/10.36897/jme/186044

Bioprinting technologies are categorized into three main types based on their physical principles: extrusion-based bioprinting (EBB), droplet-based bioprinting (DBB), and light-based bioprinting (LBB) [3]:

- EBB employs a syringe-like extruder to deposit bioink as continuous filaments through
  a needle, accommodating a wide range of bioinks with high cell densities, suitable for complex tissues.
- DBB operates like inkjet printers, using bioink composed of living cells in a hydrogel. It deposits tiny droplets using electrical, thermal, or acoustic energy, ideal for high-resolution printing and creating thin tissue layers and vascular networks.
- LBB uses laser power for precision through photopolymerization or bioink transfer, offering high cell viability and suitability for delicate structures.

EBB is the most extended family of technologies [4] because of its simpler implementation and flexibility to work with various materials. Three main actuation systems are used: pneumatic, mechanical (screw-or plunge-driven), and solenoid-based systems. Among these, pneumatic actuation systems are the most widely spread, because of their simplicity and suitability for working in sterile conditions. Most commercial solutions for bioprinting use this technology. However, this approach poses a challenge to obtain geometrically accurate constructs: the complex relation between the input pressure and the output flow of material through the needle, which is dependent of the rheological properties of the material. On top of the material flowrate in the needle, the size and shape of the filament is also dependent on printing parameters as layer height, so this relation is key to plan correctly the trajectories to bioprint a given construct. An imbalance between the expected size of the filament and the real one can lead to over-extrusion or under-extrusion. The error successively accumulates layer by layer, which leads to relatively important error in the final geometry.

Usually, the method to attain a given filament size is through trial and error. All of the printing parameters fixed except for pressure, the latter is adjusted iteratively [5]. This leads to waste of bioink, very costly per unit volume. Imprecise measuring during the initial layer might lead to unsatisfactory results with an increasing number of layers, as the error is cumulative. This phenomenon is enhanced with increasing printing precision, i.e. with smaller layer height and needle diameter. On top of issues with the control of the geometry of the filament during the extrusion, the choice of materials and printing parameters is non-trivial, as optimizing final shape fidelity as well as cell survivability often leads to opposite requirements. Two of these dualities can be identified: (i) stiff hydrogels lead to more structural integrity vs. soft hydrogels lead to higher cell viability during the extrusion as well as more cell interaction after extrusion [6], (ii) smaller extrusion needle diameter leads to higher printing precision, but this also decreases cell viability as they suffer from more shear stress during printing. Rheological models have been tested to establish a relation between input pneumatic pressure and output material flowrate [7]. A rheological test is performed to characterize the bioink, using Dynamic Mechanical Analysis (DMA). Results are then applied to a model, which predicts flowrate in function of input pressure. This method is incomplete as the relation between flowrate and filament size and shape is not straightforward given the layer height and printing speed. Furthermore, the manipulation of bioinks to perform

the DMA test can be difficult and material consuming. This is depending on the equipment used, and the cost of the equipment can be very high. In recent years, machine learning (ML) models have gained the remarkable ability to discern intricate data interactions from experimental data, enabling them to extrapolate their findings to more complex scenarios and objects where traditional handcrafted rules may not apply (long). This transformation has triggered a change in thinking towards data-driven approaches in various engineering disciplines [8]. Establishing a correlation between process parameters and quality outcomes often necessitates the derivation of empirical models, which can be accomplished using conventional statistical tools or by embracing ML techniques [9]. Consequently, data-driven machine learning algorithms, equipped with robust predictive capabilities, offer distinct advantages when it comes to predicting behaviours and exploring novel models [10].

Recent studies have shown successful applications of machine learning techniques to enhance the 3D printing of biomaterials [11–15]. In these studies, ML has been employed for three main purposes:

1. Predicting and optimizing printing parameters [16], aiming to maximize the structural properties of the printed biomaterials,
2. Material printability optimization, i.e. studying suitable rheological properties which result in better printability [17] and
3. Quality assessment of prints, to identify defects or imperfections in the printed construct [18].

In this paper, an open-loop control system using a ML model is proposed, consisting of an initial training phase, which uses a relatively low quantity of material (1 mL per 100 filaments approximately) and generates a precise model capable of predicting the output size and shape of the filament for a given material. It uses little supplementary material (two cameras) and can be applied to a large set of EBB techniques, including Micro-extrusion Bioprinting and FRESH [19]. A highly automatized protocol has been accomplished through the development of software communicating with all the instruments involved, which makes possible to attain a high cadence of data production (140 filaments created and analysed per hour). This allows the system to remain profitable in producing a high-quality ML model with little time investment. The model and is directly applicable after computing and can be extended afterwards to a wider range of printing parameters. Section 2 of this paper presents the state of the art in two fields: measuring techniques in the scope of bioprinting and Machine Learning models. Section 3 presents materials, methods, and approaches that the authors used to collect data and train the model, showing an implementation of this open-loop control system, as well as results following the application of each method. Finally, Section 4 discusses conclusions and perspectives.

2. STATE OF THE ART

2.1. GEOMETRY MEASUREMENT

Geometry measurement in bioprinting has its own challenges given the specific constraints of the domain: (i) soft and thermally sensitive materials and (ii) sterility needs to

be preserved to ensure the correct development of living cells. Thus, non-invasive measuring methods need to be implemented. Many techniques have been used to achieve this, which go from 2D imagery, which allows to measure geometry from a 2D perspective, to scanning, which allows the direct reconstruction of 3D shapes. Some of these techniques are listed below:

- Common optical sensors include high-speed cameras, pyrometers, in-line cameras, and in-line photodetectors [20]. These optical sensors can provide great insight into each layer, but are limited to observing only the surfaces.
- Optical coherence tomography (OCT) is an imaging technique that uses low-coherence light to capture micrometer-resolution, 2D- and 3D-dimensional images from within optical scattering media (e.g., biological tissue). OCT has recently been proposed to provide sub-surface information regarding the printed part [21, 22].
- Magnetic resonance imaging (MRI) is a 3D imaging technique that offer a high measurement depth for monitoring and characterizing heterogeneous soft (hydrated) materials at ambient conditions [23].
- Ultrasonic sensors have been used to detect subsurface defects by sending ultrasonic waves [24, 25].

For the purpose of the system to be implemented in this paper, common optical sensors and more precisely cameras are an optimal choice, because of their ease of integration and capacity to detect edges on any kind of material (provided an adequate background). To overcome the limitation of recovering only 2D geometry, multiple views can be used to measure different dimensions, although full 3D surface reconstruction remains out of scope.

2.2. PHYSICAL MODELS

Many physical models based on the rheology of the bioinks have been developed. Bioinks are usually modelled as shear-thinning fluids, which enables to deduce the equation of the flow through the extrusion needle and thus estimate the size of the printed filament, as for example, in the Ostwald-de Waele model [7]. These models have been proven precise within bounded operating limits but may struggle to properly predict results in atypical operating conditions (for instance, with high pressures) [26]. In addition, as these models only predict flow through the extrusion needle, they do not provide information about the shape of the filament once extruded as it is affected by gravity. This information is key as EBB techniques build layer by layer, so it is the precise knowledge of final filament shape that allows for overall high printing precision.

2.3. MACHINE LEARNING METHODS

Numerical models can be an alternative to guide the experimentations and drastically reduce the numbers of trials for optimizing the parameters. Yet, such numerical models do not exist. Hence, a methodology is proposed to build a numerical direct model predicting the shape and size of a filament for a given set of parameters. This model is data-driven, based

on a set of experiments and can predict any new combination of parameters. This way, once calibrated, no more experiments would be required to investigate the best sets of parameters for a desired filament result. For data-driven modelling, Artificial Intelligence, and especially Machine Learning in this context, is the numerical tool to be used. Indeed, a non-linear multi-parametric model can be performed, relating inputs and outputs. Once the relations found based on data points, the model can be queried for a new set of parameters to be tested and answers in real-time. The studied data points used for training the model are in this case the experiments parameters and a photo of the result filament.

Once this direct model validated, an inverse model can be built for the final objective. Indeed, in use the numerical model must advise the experiment with optimal process parameters based on a target geometry.

3. MATERIALS, METHODS, AND RESULTS

3.1. EXPERIMENTAL SETUP AND MATERIALS

The experimental setup consists of the following elements (cf. Fig. 1):

- **Bioprinter**: This is a self-developed prototype in the lab. It is a Cartesian machine with three axes. A linear motor (Parker, MX80LS) drives each axis (with approximately a 140 mm travel and a precision of 0.1 μm). The Z-axis moves the syringe holder vertically, while the x and y-axes move the platform. An MC405 motion controller (Trio Motion Technology) controls the axes. It uses an ARM11 processor. Both the platform and the syringe holder are thermo-regulated with two independent water circuit run by mini-chillers (0 to 100°C) (Huber, Minichiller 300 OLÉ).
- **Pressure controller**: an Ultimus V (Nordson) controller controls pneumatic pressure in the syringe. It provides high-precision benchtop fluid dispensing control (1 mbar precision, up to 5 bar of pressure). With a serial interface, the Ultimus V provides full electronic control of dispense time and pressure settings.
- **Printing area**: The bioprinter is assembled inside a microbiological safety hood that provides a vertical laminar flow, limiting sample contamination when working with cells and living material. A support structure has been designed for easy placement of glass slides on which lines are printed. It also provides suitable lighting conditions for capturing the filament's contour from horizontal and vertical perspectives.
- **Printing support**: filaments are printed on top of glass slides, which are single-used. A piece of paper is glued on the printing surface to provide a homogeneous background in the photos from which the geometry will be retrieved.
- **Bioink**: Pluronic® F-127 (Merck, P2443-250G) is used at a 25% w/v concentration as testing hydrogel. It is an artificial polymer, usually used as scaffolding material in bioprinting, which is stiffer at higher temperatures. The hydrogel is prepared diluting the proper amount of Pluronic powder within de-ionized water at low temperatures (4°C). Blue food coloring is added in the end to better visualize the filament in images (1 droplet/ 5 ml). The hydrogel is centrifuged at low temperatures to extract air

bubbles generated during mixing. A non-cell-laden bioink has been used for simplicity, but the same method is applicable for living cell-laden bioinks.

- **Syringe and needle**: the hydrogel was placed inside a 10cc syringe (Nordson, P/N: 7012114) connected to the pressure controller through an adapter assembly (Nordson, P/N: 7012239). Straight stainless steel needle of 0.2 mm ID, 0.42 mm OD and 12.7 mm length (Nordson, P/N: 7005008) were used during the experiments showed in this paper.
- **Cameras**: two different microscopic cameras (Dino-Lite, AM7915MZTL and AM7115MZTW) are mounted horizontally and vertically with respect to the printing plane on the bioprinter chassis. They offer high-resolution as well as a high focal length, which allows getting high-detail images at a distance.
- **Software**: A PC hosts a C++ console program offering control over both cameras, the motion controller, and the pressure controller. It takes as input a .csv file with parameters assigned to each filament and guides the operator through experiment initial preparations (camera and extrusion needle calibration, material purge) and verification. It sequentially performs each experiment, requiring the operator to replace the glass slide in each iteration and to verify the extruded line.

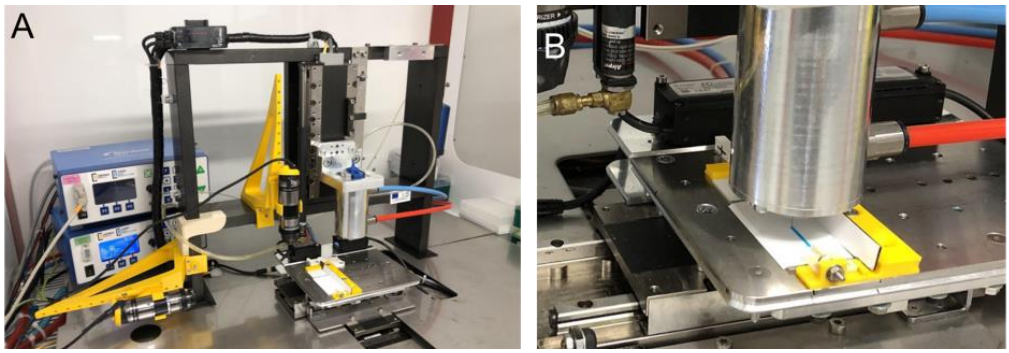

Fig. 1. A – Experimental setup within the bioprinter hood. The bioprinter *Z*-axis, (center) is mounted on the chassis (center). The *X*- and *Y*-axis are mounted under the buildplate (bottom). The vertical (left, yellow) and horizontal (center, yellow) camera supports fixed on the chassis. The printhead (center) with a syringe of bioink is fixed to the *Z*-axis. The glass slide support (bottom front, yellow) is mounted onto the buildplate. The pressure controller (left back, blue and white) is connected to the syringe through a pressure pipe. B – Detail of the bioprinter while extruding a filament

3.2. EXPERIMENTAL PROTOCOL

The successful implementation of extrusion-based bioprinting (EBB) relies on precise control of several operational parameters. These parameters include extrusion pressure or velocity, nozzle geometry (which can be either cylindrical or conical with a specified convergence angle), nozzle diameter, cartridge temperature, platform temperature, advance speed of the printhead in both the x and y-directions, and path-height and path-space. Each of these parameters plays a crucial role in determining the bioprinting process's outcome [20–22]. During the preparation of each experiment, the parameters to be set for each line to be printed in the essay are recorded in a table. The adjustable parameters are three: (i) needle height relative to the printing surface, (ii) advance speed and (iii) applied pneumatic pressure.

Other parameters that are not variable but are measured or controlled include the head of the printer's temperature, ambient temperature, bioprinter acceleration, needle diameter, needle length, and bioink type. The selected bioink temperature for this set of experiments is 30°C.

The protocol runs as follows (cf. Fig. 2):

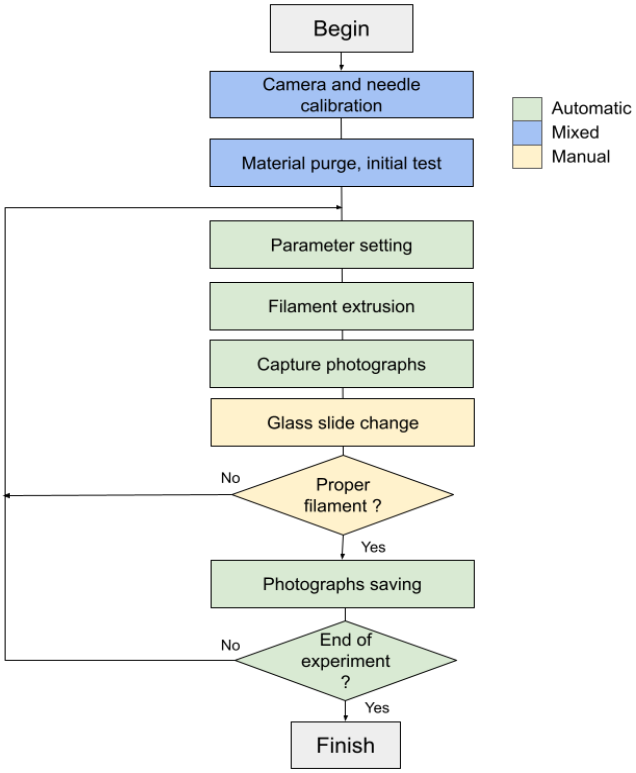

Fig. 2. Experimental protocol

- **Preparation**: A syringe full of material, and the desired needle mounted is attached to the bioprinter. The head of the printer's temperature is manually adjusted and left during 20 min to achieve thermal equilibrium inside the hydrogel. A glass slide is placed on the printing area, and the program is launched. An absolute reference inside the printing area allows camera calibration before the start of the experiment. Additionally, a second reference is placed next to the extruded line to serve as a reference in each photo. A material purge is performed to remove any air bubbles trapped in the needle. Finally, a test line is printed to verify that the preparation has been carried out correctly.
- **Sequential filament printing:** For each line, the machine approaches the starting position. Horizontal displacement begins simultaneously with the activation of pressure, which is deactivated upon reaching the end of the trajectory of a total length of 20 mm. The velocity profile is trapezoidal, meaning there is constant acceleration and deceleration until the desired velocity is achieved. Subsequently, the needle is vertically retracted, and the plate is moved to the position where horizontal and vertical photographs are taken simultaneously. Finally, the plate is moved to a position where the current glass slide can be easily removed. The operator can then

request the repetition of the printing if anomalies (such as air bubbles) are detected or proceed with the next experiment once the plate has been changed. The horizontal and vertical images are then automatically saved.

- **Ending**: once all the filaments have been printed, the program stops and automatically outputs a data file relating each photograph with its corresponding set of parameters.

3.3. TEST SELECTION

It is possible that for a given set of printing parameters, the flowrate is not sufficient (known as under-extrusion) and thus a non-continuous filament is obtained. This situation is to be avoided as the model is intended to predict the width and height of a continuous filament. In order to optimize the number of tests that are useful as input data, a prior test selection with a high probability of being continuous is carried out. For this purpose, an initial set of tests has been run in a very wide range of parameters, which will surely have a considerable number of non-continuous filaments. The classification of each filament as continuous or discontinuous is associated with the values of the process parameters, which allows the construction of a Logistic Regression Model (LRM): $f(z) = \frac{1}{1+e^{-z}}$, with $z = A + Bp + Cv + Dh$, p being the pressure expressed in bars, v the speed expressed in mm/s and h the needle height with respect to the printing surface expressed in mm, and A, B, C and D the parameters of the model. The resulting LMR predicts the probability (from 0 to 1) of a filament being continuous given a set of input parameters. This model is applicable, therefore, for making informed decisions about configuring parameters in filament printing experiments.

A series of prior longitudinal filament printing tests (154 in total) have been conducted, involving the wide-ranging variation of different process parameters and variables, and observing the production of continuous or discontinuous filaments. The resulting LRM is the following: $f(z) = \frac{1}{1+e^{-z}}$, with $z = -4.3 + 2p - 0.1v - 0.3h$. The confusion matrix for the set of tests carried out with a probability threshold of 0.8, which reasonably ensures that the specific combination of parameters allows for the printing of continuous filaments, is the following (Table 1).

The graphic on the right (cf. Fig. 3) shows the line which represents the LRM model isoquant at the chosen threshold ($f(z) = 0.8$) vs the data points used to compute the model. Any filament whose parameters fall under the line is given a probability higher than 0.8 to be continuous. It is possible to conclude that the layer height has a low effect on continuity and that probability of continuity increases with pressure and decreases with velocity.

To produce a working model for the open-loop system exposed in this article, the geometry of each filament needs to be retrieved. This quantity of interest is usually measured manually (approximative width and height) or subjectively (good and bad shape). The automatization of the geometry measurement for each filament through image analysis is proposed. Indeed, the Artificial Intelligence field also includes Image Processing and Computer Vision techniques. Those methods can be applied on an image to detect an object (the deposited filament) and measure the widths and heights all along the shape.

Table 1. Confusion matrix of the test dataset applying the threshold $f(z) = 0.8$

	Negative	Positive
False	25	5
True	31	93

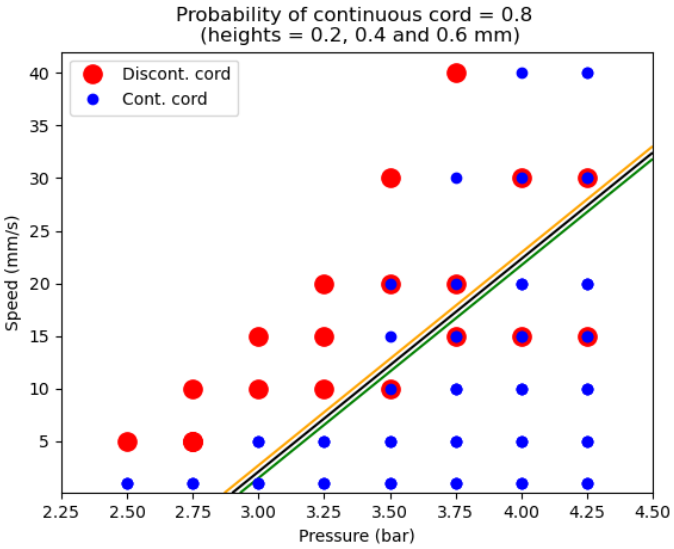

Fig. 3. Threshold of the LRM model *f(z)* = 0.8 vs data points used to compute the model

3.4. IMAGE PROCESSING

This way, the average quantity of interest (width and height) is retrieved but also its variance along the filament. Hence, it can determine whether the filament edges are regular (c.f. Fig. 4). A filament with regular edges presents a very low variance width and height when irregular edges show a very high variance.

A.  B. 

Fig. 4. A. – Filament with regular edges; B. – Filament with irregular edges

Photographs of the result filaments are automatically taken during the experiment from the side and from above (c.f. Fig. 5) to compute respectively the height and the width.

A. 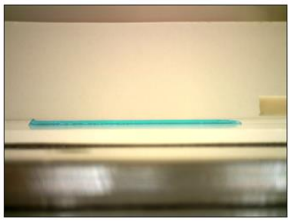 B. 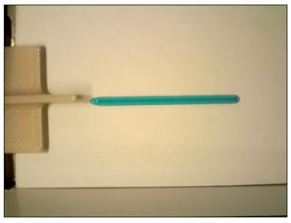

Fig. 5. Photo of the filament automatically shot at the end of the process from the A. side and from B. above

Based on the dye color, a HSV (Hue Saturation Value) conversion helps filtering the pixels in the image and approximatively detect the filament location (c.f. Fig. 6).

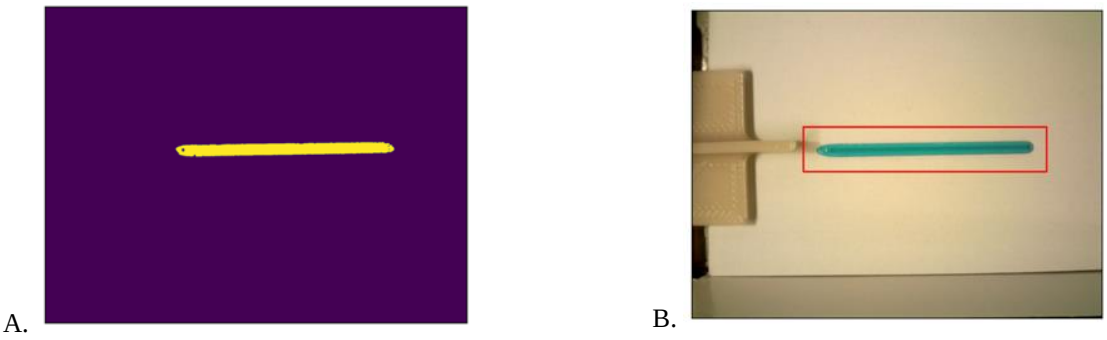

Fig 6. HSV encoding of the photo from above the filament: A. – Binary image filtered, B. – Approximative location of the filament in the image

Once the approximative location computed, only the filament remains on the cropped image. Therefore, the only remaining edges are those of the filament. Using the Canny edges detection with the scikit-image library in Python [27], all pixels around the filament can be retrieved (cf. Fig. 7). From those pixels' coordinates, the width and the height along the filament can be computed (c.f. Fig. 8). Horizontal and vertical images provide a resolution of 11 µm and 15 µm per pixel, respectively.

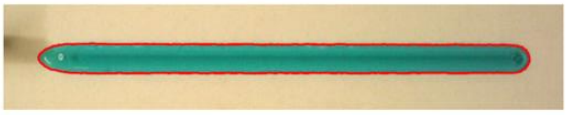

Fig. 7. Filament edges detected with Canny method [27] on the cropped image

Fig. 8. A. – Width and B. – Height automatically computed along the printed filament with image processing

This approach automatizes the measure of the filament with more consistent and relevant information extraction. Thus, a database relating the process parameters ("Inputs" in Table 2) with those quantities of interest ("Outputs" in Table 2) is built.

Table 2. Dataset header with process parameters (inputs) to relate with quantities of interest (outputs)

INPUTS			OUTPUTS			
Pressure	Advance Speed	Nozzle Height	Width Average	Width Variance	Height Average	Height Variance

This dataset counts 420 filaments (140 distinct parameter combinations repeated 3 times) is used for creating a data-driven manifold described in next section.

3.5. MACHINE LEARNING FOR MANIFOLD PREDICTIONS

The objective of this section is to create a manifold of the filament dimensions depending on the process parameters. This approach is data-driven, based on the experimental results, and modeled using a Machine Learning algorithm. Thus, a direct model is created, predicting the filament dimensions and shape from any process parameters queried. For the data-driven Machine Learning, the Support Vector Machine (SVM) [28, 29] fits the requirements for non-linearity and data sparsity. Indeed, with three parameters involved in the process (Pressure, Advance Speed and Nozzle Distance), Deep Learning algorithms like Neural Network Regressor, would require much more than 420 distinct parameter combinations [30, 31]. Fitting the 420 points available with Machine Learning built a manifold surface for each of the studied outputs (Width Average, Width Variance, Height Average, Height Variance). This is the direct model. The SVM algorithm was first conceived for classification problems, i.e. for separating samples into classes. The algorithm computes by iterations a hyperplane with a margin whose objective is to separate at best the training points available. This margin is built to be the largest possible and containing the minimum number of training points. As this relation here is not linear, this cannot be obtained in the original space. Therefore, the idea of the SVM algorithm is to find a higher dimensional space where this margin can be linear, using a kernel application. In our case, a non-linear Radial Basis Function is used: $(x, y) \mapsto (x, y, z)$, with $z = \exp(-\gamma(x^2 + y^2))$.

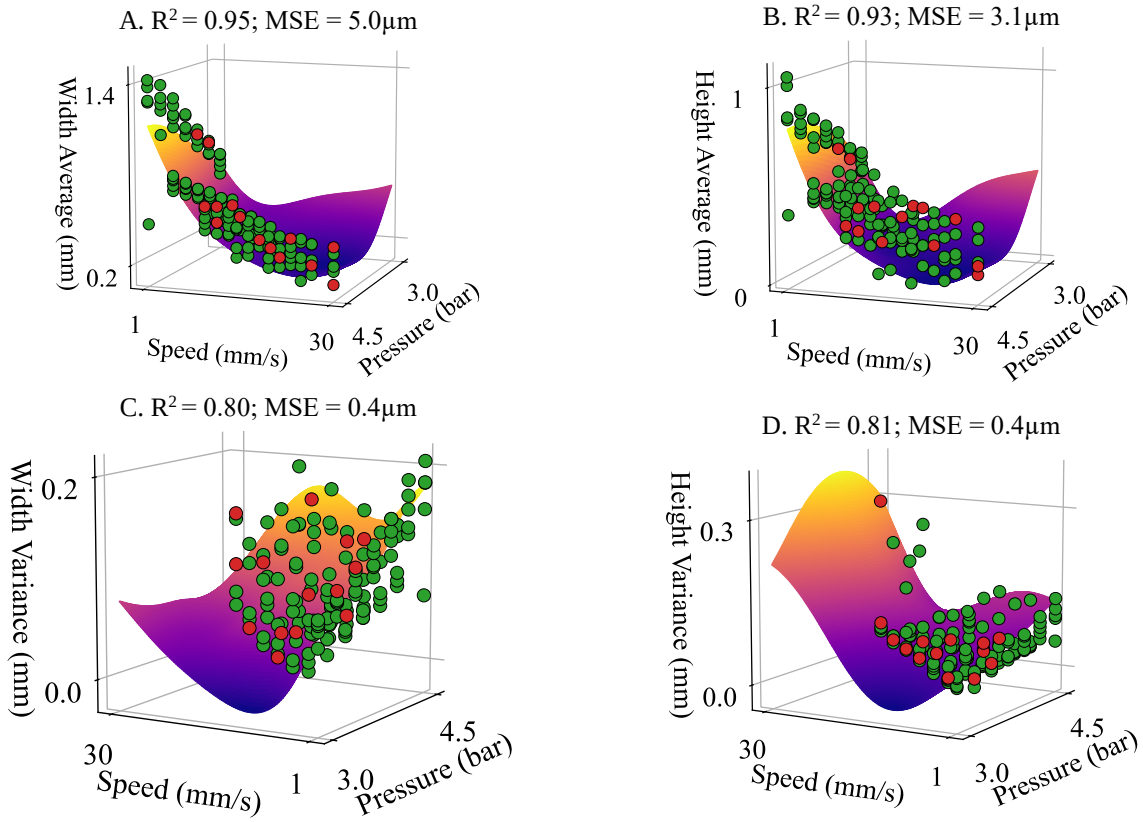

Fig. 9. Data-driven manifolds computed with SVM regressor for A. Width Average, B. Height Average, C. Width Variance, D. Height Variance, for Nozzle Height = 0.2 mm

This classification method is extended to solve regression problems where the objective is to predict a scalar rather than a class. The manifolds for each quantity of interest are presented in Fig. 9. On these plots, the points represent the experimental data used to train the SVM model in green (90% of the experimental data). The red points represent the experimental data used to validate the model (10% of the experimental data). The R^2 score and the Mean Square Error (MSE) results are given for each manifold, presenting a good prediction accuracy.

With these manifolds of the direct model, the filament shape can be predicted for any set of parameters.

3.6. STOCHASTIC MACHINE LEARNING MODELS

The experimental context involves an issue with repeatability. Indeed, with the same process parameters, different results might be obtained, depending on the bioink. A metric for this geometric repeatability is need. The same set of parameters has been repeated three times and the filament measure the same way as previously. Therefore, the variance of the average width and height between those three repetitions can be measured. The higher the variance, the less repeatable the experiment was. The final objective will be there to predict numerically the repeatability of one experiment before running it. The same way as in the previous section, a SVM model is built to predict such metrics. The results are presented in Fig. 10. The higher the score, the less repeatable the combination of parameters.

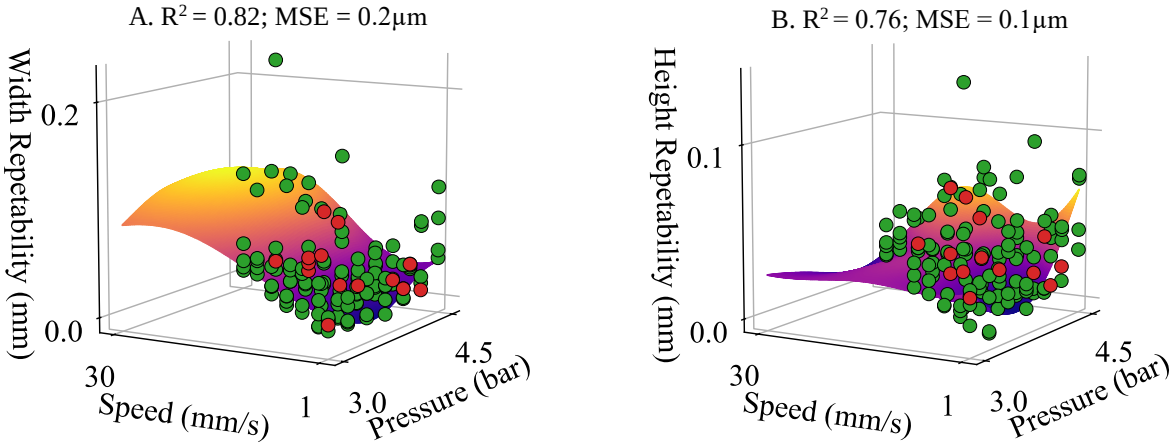

Fig. 10. Data-driven manifolds computed with SVM regressor for A. Width Repeatability, B. Height Repeatability, for Nozzle Height = 0.2 mm

Two direct models have been built to predict the width, height, and repeatability for any given combination of parameters. This way, before testing by experimentation a new set of process parameters, it can be tested numerically to get the results in real-time. If the numerical answer is acceptable, the experiment can be led. However, a better use of this manifold is for the numerical model to lead the experiment and advice a combination of parameters to run for a targeted geometry. This is presented in the next section.

3.7. INVERSE MODEL FOR PARAMETERS OPTIMIZATION

For the numerical manifold to advice parameters for a targeted width and height, the direct model is queried in a range of parameters to optimize those quantities of interest. Thus, from the direct model built with the SVM algorithm, an inverse model is built here minimizing the difference between the predicted width and height on the one hand and target width and height on the other hand. This approach can retrieve multiple sets of possible parameters. This can be sorted or filtered using the repeatability model to assure the consistency of the experiment. This inverse model is presented in Fig. 11.

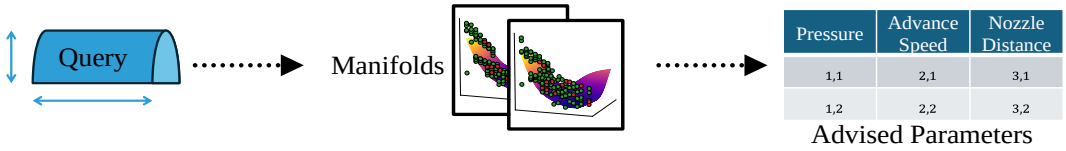

Fig. 11. Inverse model based on the manifolds predicted using the Machine Learning direct model to advice optimal sets of process parameters

4. CONCLUSIONS AND PERSPECTIVES

This new numerical approach involving Machine Learning to lead experiments with optimal choice of process parameters shows promising result. It has been applied here in the context of bioprinting with three main parameters (Pressure, Advance Speed and Nozzle Height) with satisfying geometry predictions. An open-loop control system has been built this way by the automatization of (i) capturing photos of the printed cord (ii) computing its actual geometry with image processing (iii) advising in real-time optimal parameters with an inverse model based on Machine Learning. Specifically, a small quantity of bioink (under 5 ml) has been used to print a series of 420 filaments in a semi-automatic setup. This data has been used to automatically compute a high accuracy Machine-Learning model ($R^2 > 0.91$) covering three key printing parameters in a wide range. This enables to advice printing parameters that produce a filament of specific size with a mean squared error of 5.0 μm for the width and 3.1 μm for the height of the filaments.

In conclusion, the following step would be to take advantage of this real-time approach to compute optimal parameters during the bioprinting [32] with a closed-loop control [33]. Indeed, a deviation can be automatically detected between the printed bead and the target geometry with the steps (i) automatic captures and (ii) image processing. From this deviation, an optimal set of parameters can be advised to correct the continuation of the printing.

This will be validated in a closed-loop perspective with experimental data with objective of real-time in-process correction.

REFERENCES

[1] FERRARI A., FRANK D., HENNEN L., et al., 2018, *Additive Bio-Manufacturing: 3D Printing for Medical Recovery and Human Enhancement*, European Parliamentary Research Service *(EPRS)*, Report Number: PE 614.571.

[2] HE Y., GAO Q., JIN Y., 2022, *Cell Assembly with 3D Bioprinting*, Wiley-VCH.
[3] NEAGU A., 2023, *Towards 4D Bioprinting*, Academic Press, Elsevier Inc., London.
[4] SANTONI S., GUGLIANDOLO S.G., SPONCHIONI M., MOSCATELLI D., COLOSIMO B.M., 2021, *3D Bioprinting: Current Status and Trend – a Guide to the Literature and Industrial Practice*, Bio-Design and Manufacturing, 5, 14–42, https://doi.org/10.1007/s42242-021-00165-0.
[5] GILLISPIE G., PRIM P., COPUS J., FISHER J., MIKOS A.G., YOO J.J., ATALA A., LEE S.J., 2020, *Assessment Methodologies for Extrusion-Based Bioink Printability*, Biofabrication, 12/2, 022003, https://doi.org/10.1088/1758-5090/ab6f0d.
[6] BOTT K., UPTON Z., SCHROBBACK K., EHRBAR M., HUBBELL J.A., LUTOLF M.P., RIZZI S.C., 2010, *The Effect of Matrix Characteristics on Fibroblast Proliferation in 3D Gels*, Biomaterials, 31/32, 8454–8464, https://doi.org/10.1016/j.biomaterials.2010.07.046.
[7] SCHWAB A., LEVATO R., D'ESTE M., PILUSO S., EGLIN D., MALDA J., 2020, *Printability and Shape Fidelity of Bioinks in 3D Bioprinting*, Chem. Rev. 120, 11028–11055, https://doi.org/10.1021/acs.chemrev.0c00084.
[8] NG W.L., CHAN A., ONG Y., CHUA C., 2020, *Deep Learning for Fabrication and Maturation of 3D bioprinted Tissues and Organs*, Virtual and Physical Prototyping, 15, 1–19, https://doi.org/10.1080/17452759.2020.1771741.
[9] VERHEYEN C., UZEL S., KURUM A., ROCHE E., LEWIS J., 2023, *Integrated Data-Driven Modelling and Experimental Optimization of Granular Hydrogel Matrices*, Matter, 6, 1–22, https://doi.org/10.1016/j.matt.2023.01.011.
[10] CHATURVEDI M., VENDAN S.A., 2022, *Data-Driven Models in Machine Learning: an Enabler of Smart Manufacturing*, Big Data Analytics in Smart Manufacturing, P. Suresh, T. Poongodi, B. Balamurugan and M. Sharma (Eds.), 35–68, Chapman and Hall-CRC.
[11] YU C., JINGCHAO J., 2020, *A Perspective on Using Machine Learning in 3D Bioprinting*, International Journal of Bioprinting, 6/1, 253, https://doi.org/10.18063/ijb.v6i1.253.
[12] MALEKPOUR A., CHEN X., 2022, *Printability and Cell Viability in Extrusion-Based Bioprinting form Experimental, Computational, and Machine Learning Views*, Journal of Functional Biomaterials, 13.
[13] SUN J, YAO K., AN J., JING L., HUAN K., HUANG D., 2023, *Machine Learning and 3D Bioprinting*, International Journal of Bioprinting, 9/4, 717, https://doi.org/10.18063/ijb.717.
[14] NING H., ZHOU T., JOO S., 2023, *Machine Learning Boosts Three-Dimensional Bioprinting*, International Journal of Bioprinting, 9/4, 739, https://doi.org/10.18063/ijb.739.
[15] VENKATA KRISHNA D., MAMILLA R.S., 2023, *Machine Learning-Assisted Extrusion-Based 3D Bioprinting for Tissue Regeneration Applications*, Annals of 3D Printed Medicine, 12, 100132, https://doi.org/10.1016/j.stlm.2023.100132.
[16] FU Z., ANGELINE V., SUN W., 2021, *Evaluation of Printing Parameters on 3D Extrusion Printing of Pluronic Hydrogels and Machine Learning Guided Parameter*, 2021, International Journal of Bioprinting, 7/4, 434, https://doi.org/10.18063/ijb.v7i4.434.
[17] LEE J., OH S., AN S., KIM W., KIM S., 2020, *Machine Learning-Based Design Strategy for 3D Printable Bioink: Elastic Modulus and Yield Stress Determine Printability*, 2020 May 28, Biofabrication, 12/3, 035018, https://doi.org/10.1088/1758-5090/ab8707.
[18] CONEV A., LITSA E., PEREZ M., DIBA M., MIKOS A., KAVRAKI L., 2020, *Machine Learning Guided 3D Printing of Tissue Engineering Scaffolds*, Tissue Engineering, Part A, 2020 Dec. 26/23-24,1359-1368, https://doi.org/10.1089/ten.TEA.2020.0191.
[19] SHIWARSKI D.J., HUDSON A.R., TASHMAN J.W., FEINBERG A.W., 2021, *Emergence of Fresh 3D Printing as a Platform for Advanced Tissue Biofabrication*, APL Bioeng. 5/1. 010904, https://doi.org/10.1063/5.0032777.
[20] ARMSTRONG A., PFEIL A., ALLEYNE A., WAGONER JOHNSON A., 2021, *Process Monitoring and Control Strategies in Extrusion-Based Bioprinting to Fabricates Partially Graded Structures*, Bioprinting 21, e00126, https://doi.org/10.1016/j.bprint.2020.e00126.
[21] YANG S., CHEN Q., WANG L., XU M., 2022, *In-Situ Defect Detection and Feedback Control with Three-Dimensional Extrusion-Based Bioprinter-Associated Optical Coherence Tomography*, International Journal of Bioprinting 9/1, 624, https://doi.org/10.18063/ijb.v9i1.624.
[22] YANG S., WANG L., CHEN C., XU M., 2021, *In-Situ Process Monitoring and Automated Multi-Parameter Evaluation Using Optical Coherence Tomography During Extrusion-Based Bioprinting*, Additive Manufacturing, 47, 102251, https://doi.org/10.1016/j.addma.2021.102251.
[23] SCHMIEG B., GRETZINGER S., SCHUHMANN S., GUTHAUSEN G., HUBBUCH J., 2022, *Magnetic Resonance Imaging as a Tool for Quality Control in Extrusion-Based Bioprinting*, Biotechnology Journal, 17/5, e2100336, https://doi.org/10.1002/biot.202100336.
[24] CHANSORIA P., SHIRWAIKER R., 2019, *Characterizing the Process Physics of Ultrasound-Assisted Bioprinting*, Scientific Reports, 9, 1–17, 13889, https://doi.org/10.1038/s41598-019-50449-w.

[25] RULAND A., GILMORE K.J., DAIKUARA L.Y., FAY C.D., YUE Z., WALLACE G.G., 2019, *Quantitative Ultrasound Imaging of Cell-Laden Hydrogels and Printed Constructs*, Acta Biomaterialia, 91, 173–185, https://doi.org/10.1016/j.actbio.2019.04.055.

[26] EMEBU S., OLABANJI OGUNLEYE R., ACHBERGEROVA E., VITKOVA L., PONIZIL P., MENDOZA MARTINEZ C., 2023, *Review and Proposition for Model-Based Multivariable-Multiobjective Optimisation of Extrusion-Based Bioprinting*, Applied Materials Today, 34, 101914, https://doi.org/10.1016/j.apmt.2023.101914.

[27] CANNY J., 1986, *A Computational Approach to Edge Detection*, IEEE Transactions on pattern analysis and machine intelligence, 6, 679–698, https://doi.org/10.1109/TPAMI.1986.4767851.

[28] SMOLA A.J., SCHÖLKOPF B., 2004, *A Tutorial on Support Vector Regression*, Statistics and Computing, 14, 199–222, https://doi.org/10.1023/B:STCO.0000035301.49549.88.

[29] BISHOP C.M,, 2010, *Pattern Recognition and Machine Learning*, Chapter 7 Sparse Kernel Machines.

[30] TANGE R.I., RASMUSSEN M.A., TAIRA E., *et al.*, 2017, *Benchmarking Support Vector Regression Against Partial Least Squares Regression and Artificial Neural Network: Effect of Sample Size on Model Performance*, Journal of Near Infrared Spectroscopy, 25/6. 381–390, https://doi.org/10.1177/0967033517734.

[31] CASTERAN F., DELAGE K., HASCOËT N., *et al.*, 2022, *Data-Driven Modelling of Polyethylene Recycling Under High-Temperature Extrusion*, Polymers, 14/4, 800, https://doi.org/10.3390/polym14040800.

[32] HASCOËT J.Y., ROSA B., DE VILLEMAGNE P., HALARY F., 2017, *Modeling of 4D-Bioprinting Process for Improved Final Resolution of a Tissue*, Conference: 3D Bioprinting in Cancer Research, Nantes.

[33] HASCOËT J.Y., CHABOT A., RAUCH M., 2017, *Towards Closed Loop Control for Additive Manufacturing*, Conference on Welding and Additive Manufacturing, Metz, France.